Acta Crystallographica Section B
Structural Science
ISSN 0108-7681

The natural tiling approach to cation conductivity in $KAlO_2$ polymorphs

Vladimir I. Voronin,[a] Georgi Sh. Shekhtman[b] and Vladislav A. Blatov[c]*

[a]Institute of Metal Physics Urals Branch RAS, S.Kovalevskoy Street 18, 620041 Ekaterinburg, Russian Federation, [b]Institute of High Temperature Electrochemistry Urals Branch RAS, S.Kovalevskoy Street 22, 620990 Ekaterinburg, Russian Federation, and [c]Samara State University, Ac. Pavlov Street 1, 443011 Samara, Russian Federation

Correspondence e-mail: blatov@ssu.samara.ru

Received 11 March 2012
Accepted 17 June 2012

A detailed analysis of correlations between structural features and cation conductivity is performed for $KAlO_2$ polymorphs in a wide temperature range of 300–1023 K. To explore the migration maps of K^+ cations we have used neutron diffraction data for low- and high-temperature $KAlO_2$ polymorphs and applied for the first time a novel algorithm based on the natural tiling concept and implemented it into the program package *TOPOS*. Five independent elementary channels for the K^+ cation migration have been revealed whose cross-sections were found to be essentially different in the low-temperature form, indicating a high anisotropy of the cation conductivity. During the transition to the cubic high-temperature phase all five channels become equivalent with sharply increased cross-sections that account for the jump-like increase of the cation conductivity and gives rise to its three-dimensional character.

1. Introduction

The last 30 years featured an intensive search for new alkali ion-conducting solid electrolytes and, as a result, a large number of compounds with high alkali cation conductivity have been synthesized (Burmakin, 1992; West, 1995; Avdeev *et al.*, 2009). Besides widespread Li^+ and Na^+ conducting materials, close attention has been drawn to solid electrolytes with mobile heavy alkali cations, in particular K^+. One of the promising classes of K^+ cation conductors are solid solutions based on potassium metaaluminate, $KAlO_2$ (Burmakin, 1992; Avdeev *et al.*, 2009).

The first X-ray crystal structure data on potassium metaaluminate were published by Brownmiller (1935) who interpreted the crystal structure of $KAlO_2$ as face-centered cubic (f.c.c.) with a = 7.68 Å, space group $Fd\bar{3}m$. Then Barth (1935) supposed that the room-temperature modification of $KAlO_2$ is similar to cristobalite. Later Burmakin *et al.* (1978) found that $KAlO_2$ undergoes a first-order phase transition at 810 K and the f.c.c. cell determined by Brownmiller should be assigned to the high-temperature form of $KAlO_2$, while low-temperature $KAlO_2$ being stable below 810 K has a primitive cubic cell with a doubled parameter a = 15.41 Å. Husheer *et al.* (1999) and Sokolowski & Kotarba (2000) refined the low-temperature form of $KAlO_2$ as orthorhombic, space group *Pbca*, with a:b:c $\simeq$ 1:2:3; Vielhaber & Hoppe (1969) and Pistorius & de Vries (1973) assigned it to the $KGaO_2$ structure type. According to Sokolowski & Kotarba (2000), $KAlO_2$ becomes cubic above 773 K which slightly differs from the results of Burmakin *et al.* (1978). De Kroon *et al.* (2001) reported the orthorhombic low-temperature form $KAlO_2$ with a = 4.280, b = 8.901, c = 5.466 Å and tetragonal form between 873 and 1573 K, which transforms into the cubic form at 1573 K. Finally, the neutron

Table 1
Crystallographic data for $KAlO_2$ phases at different temperatures.

T (K)	Space group, Z	Cell parameters (Å), V (Å^3)	θ_{max}, R_{int}	R, wR, N_{ref}, N_{par}
300	*Pbca*, 8	5.4387 (2), 10.9236 (3), 15.4564 (4), 918.26 (5)	164.6, 0.025	0.013, 0.017, 566, 68
400	*Pbca*, 8	5.4457 (3), 10.9401 (7), 15.4698 (9), 921.6 (1)	164.8, 0.032	0.044, 0.057, 569, 70
500	*Pbca*, 8	5.4560 (4), 10.9617 (8), 15.489 (1), 926.4 (1)	164.8, 0.039	0.047, 0.061, 573, 70
600	*Pbca*, 8	5.4668 (4), 10.9862 (9), 15.510 (1), 931.5 (1)	164.8, 0.044	0.045, 0.058, 574, 70
700	*Pbca*, 8	5.4788 (5), 11.012 (1), 15.536 (2), 937.4 (2)	164.8, 0.059	0.047, 0.059, 577, 70
773	*Pbca*, 8	5.4888 (2), 11.0346 (4), 15.5598 (5), 942.40 (6)	164.8, 0.060	0.030, 0.038, 579, 66
833	$Fd\bar{3}m$, 4	7.8033 (6), 475.16 (7)	164.8, 0.115	0.060, 0.078, 24, 26
923	$Fd\bar{3}m$, 4	7.8179 (5), 477.83 (5)	164.8, 0.032	0.046, 0.061, 24, 32
1023	$Fd\bar{3}m$, 4	7.8329 (3), 480.58 (4)	164.8, 0.043	0.026, 0.035, 24, 32

powder diffraction study of undoped $KAlO_2$ (Burmakin *et al.*, 2004) and the solid solutions $K_{1-x}Al_{1-x}Ti_xO_2$ (Burmakin *et al.*, 2005) confirmed the data published by Husheer *et al.* (1999) and Sokolowski & Kotarba (2000).

A similar cristobalite-like framework of AlO_4 tetrahedra were found in $MAlO_2$ (M = Li, Na, Rb, Cs; Marezio, 1965; Bertaut *et al.*, 1965; Kaduk & Pei, 1995; Langlet, 1964), however, these compounds are not isostructural to $KAlO_2$. Detailed structural data over the wide temperature region for ferrites $AFeO_2$ (A = K, Rb and Cs) which are isostructural to $KAlO_2$ are presented by Ali *et al.* (2010), Sheptyakov *et al.* (2010) and Müller *et al.* (2010).

The three-dimensional framework in both $KAlO_2$ polymorphs is composed of corner-shared AlO_4 tetrahedra. Experimentally determined Al—O distances in the room-temperature modification (Voronin *et al.*, 2010) are close to the sum of the Al^{3+} and O^{2-} radii (Shannon, 1976), therefore, AlO_4 tetrahedra are almost regular. There are rather large voids of two types in the framework where two non-equivalent K^+ cations surrounded by eight O^{2-} anions are located. The average K—O distances in both coordination polyhedra [$\langle$K1—O$\rangle$ = 2.987 (3), $\langle$K2—O$\rangle$ = 2.974 (2) Å] exceed the sum of the K^+ and O^{2-} radii (2.91 Å). This fact along with the large experimental value of the Debye–Waller factor for potassium ions ($W \simeq 1.1$ Å^2) indicates that the K—O bonds are rather weak, consistent with the enhanced mobility of the K^+ cations.

In none of these papers were the relations between the crystal structure features and the K^+ cation conductivity studied. This is true for studies of other types of cation solid electrolytes: despite rich experimental diffraction data, universal structural models of conductivity were not developed. Recently, Blatov *et al.* (2006), Anurova *et al.* (2008), Anurova & Blatov (2009) developed a new method of computer analysis of cation migration paths resting upon standard crystallographic data and the Voronoi–Dirichlet partition of the crystal space; this method was successfully tested with a large number of Li-containing compounds. Using the same approach, Voronin *et al.* (2010) analyzed the migration paths of K^+ cations in the crystal lattice of the $KAlO_2$ low-temperature form and showed an essential anisotropy of the K^+ cation conductivity.

In this paper we recheck the controversial data on the $KAlO_2$ polymorphism and consider in detail the relations between the crystal structure features and the conductivity of $KAlO_2$ within the temperature range 300–1023 K. For this purpose, we have used high-resolution neutron diffraction data and an improved method of the conductivity analysis that was implemented into the program package *TOPOS* (Blatov, 2006). *TOPOS* and the related manuals are available for free at http://www.topos.samsu.ru/.

2. Experimental

The methods of synthesis and sample preparation have been described elsewhere (Burmakin *et al.*, 1979, 2004). Neutron diffraction experiments were carried out using the high-resolution powder neutron diffractometer HRPT (SINQ Spallation source of Paul Scherrer Institute, Villigen, Switzerland; Fischer *et al.*, 2000). A $KAlO_2$ sample was placed in an evacuated vanadium container and heated up to a high temperature to remove moisture and then cooled down to room temperature at persistent evacuation. Structural parameters were refined by the Rietveld technique using the *FULLPROF* program (Rodriguez-Carvajal, 1993). When analyzing the integral intensity of peaks the radiation background was approximated by a 18-term polynomial. The neutron diffraction profile was described with the pseudo-Voigt function. The crystallographic data are given in Table 1.

Our results confirmed recently published data (Voronin *et al.*, 2010) for $KAlO_2$ at room temperature [*Pbca*, a = 5.4389 (1), b = 10.9235 (2), c = 15.4563 (2) Å]. Between room temperature and 810 K the neutron diffraction patterns are similar and may be interpreted within the model of the low-temperature phase. Above 810 K some reflections disappear, indicating the transition to a higher-symmetry structure. The neutron diffraction data for the high-temperature form of $KAlO_2$ can be indexed in a cubic cell (the $Fd\bar{3}m$ space group) that reflects a first-order transition from the orthorhombic low-temperature form to the cubic high-temperature form. The cubic phase does not undergo any transition at the subsequent temperature increase up to 1023 K. Thus, according to our data, at ordinary pressure $KAlO_2$ only has two phases which will be further referred to as low-temperature (orthorhombic) and high-temperature (cubic).

To determine migration maps (*i.e.* sets of migration paths of mobile cations within the framework) from crystallographic data, we used the program package *TOPOS* modified by Blatov *et al.* (2006) for studying fast-ion conductors. An important difference compared with our previous study of the room-temperature $KAlO_2$ phase (Voronin *et al.*, 2010) was that we used a novel algorithm based on the natural tiling concept (Anurova & Blatov, 2009) that is most applicable for compounds with rather simple framework topology. As opposed to the Voronoi–Dirichlet approach (Voronin *et al.*,

2010), the natural tiling algorithm provides simpler and easier interpretable migration maps. It is also much more stable to the geometrical distortions of the framework and results in topologically similar migration maps if the framework topology is retained after distortion. Nonetheless, this algorithm was not applied to compare in detail its results with experimental data on ionic conductivity.

Let us recall that the natural tiling of a net is an unambiguous method to subdivide an infinite framework into finite three-dimensional objects (natural tiles) that are confined by strong rings (cycles of atoms that are not sums of smaller cycles) and can be considered as generalized polyhedra, *i.e.* the polyhedra that can have curved faces and two-coordinated vertices (Fig. 1).

The framework simplicity can be assessed with the *tiling transitivity* parameter *pqrs*, where the integers *p*, *q*, *r* and *s* denote the number of non-equivalent atoms, bonds, rings and tiles in the framework: the smaller the transitivity the simpler the framework topology. Indeed, the $[AlO_2]^-$ framework has one of the simplest and highly symmetric topologies of cristobalite or diamond if one considers only Al atoms; the diamond-like framework of the highest $Fd\bar{3}m$ symmetry has the smallest possible transitivity 1111 (Blatov *et al.*, 2007), *i.e.* there is only one kind of atom, bond, ring and tile in the framework. Blatov *et al.* (2007) showed that natural tiles and their faces (strong rings) correspond to minimal cages and windows of the framework, respectively. The net whose edges connect the centers of the natural tiles and pass through the tile faces is called *dual net*; it is the net that contains the migration map for fast-ion conductors (Anurova & Blatov, 2009). There is a one-to-one relation between topological elements of the framework and its dual net; in particular, nodes and edges of the dual net correspond to cages and windows of the framework. The diamond net is *self-dual*; this means that the dual net has also the diamond topology (Fig. 2).

Every edge of the dual net corresponds to an *elementary channel*, *i.e.* to a part of the migration channels passing through a particular window (Fig. 2). In general, the migration map is a subnet of the dual net since some windows and cages are not accessible for mobile cations. The corresponding elementary channels will be *insignificant*; they should be removed resulting in the migration map that is thereby a subnet of the dual net. It is important that the number of elementary channels is always finite – it is equal to the number of non-equivalent edges of the dual net. Thus, the analysis of an infinite migration map that in general contains an infinite number of migration paths is substituted for the analysis of elementary channels.

Ordinarily, the natural tiling approach results in a simpler migration map than the method based on the Voronoi–Dirichlet partition (Anurova *et al.*, 2008; Voronin *et al.*, 2010). The point is that every framework window or cage corresponds to strictly one edge or node of the dual net while the Voronoi–Dirichlet graph often provides conglomerates of edges and vertices especially for distorted frameworks (Anurova & Blatov, 2009). This feature of the natural tiling approach is especially useful for a comparative analysis of migration maps in structurally similar frameworks that were crucial for our investigation.

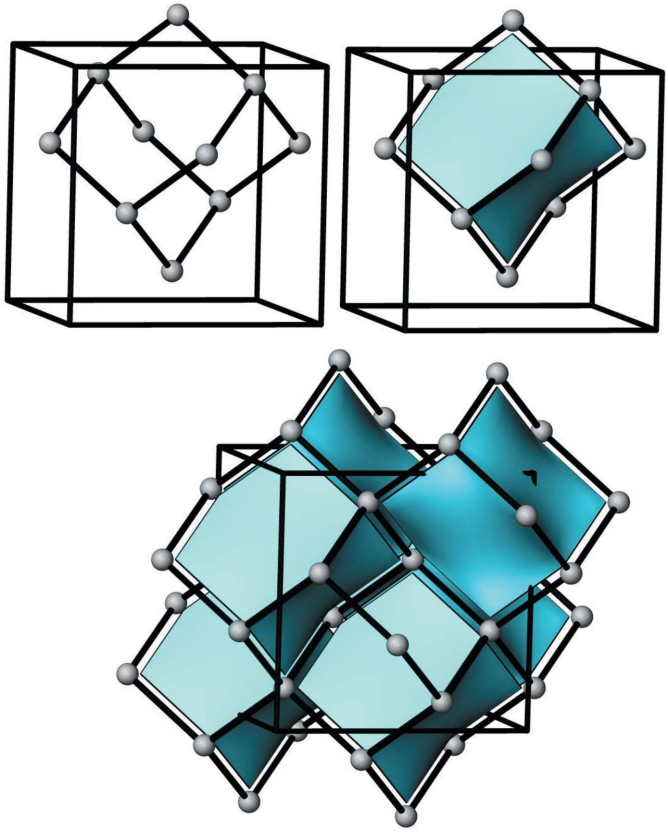

Figure 1
(*a*) Natural tiles and (*b*) tiling of a diamond net.

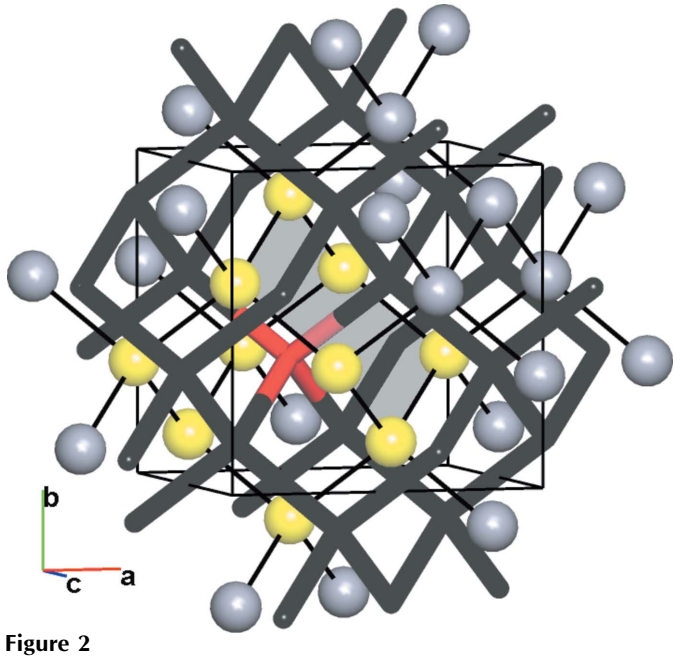

Figure 2
Diamond net (grey balls) and the corresponding dual net (black lines). A natural tile (yellow balls) confined by four 6-rings is selected in the diamond net, and the center of the corresponding cage together with four channels passing through the four windows are red. One 6-ring is shaded.

To determine the significant elementary channels, *i.e.* the windows through which the mobile cations can pass, one should apply geometrical criteria (Anurova *et al.*, 2008; Anurova & Blatov, 2009) taking into account the size of the cations and their polarizability. For potassium cations migrating through oxygen-bound windows the minimal radius of the window, *i.e.* the distance from the window center to the centers of the oxygen atoms, can be calculated as $r_{min} = (r_K + r_O)\gamma_{KO}$, where r_K and r_O are potassium and oxygen ionic radii, and γ_{KO} is the deformation factor, which reflects the polarizability of the K—O pair during migration. All elementary channels of radius smaller than r_{min} should be assumed insignificant. Voronin *et al.* (2010) estimated r_{min} as $(1.33 + 1.36) \times 0.85 \simeq 2.30$ Å, where $r_K = 1.33$ Å, $r_O = 1.36$ Å, $\gamma_{KO} = 0.85$; this r_{min} value is used in this paper.

3. Discussion

3.1. Relations between crystal structures of the $KAlO_2$ polymorphs

Ali *et al.* (2010) and Sheptyakov *et al.* (2010) showed that the phase transitions in the $AFeO_2$ (A = K, Rb, Cs) compounds whose crystal structures are similar to that of $KAlO_2$ consist of rotating tetrahedra as a whole and ordering them along a body diagonal of the unit cell. In this work we propose another approach to the description of the temperature changes in the $KAlO_2$ crystal structure that yields a deeper insight into the phase transition mechanism. The orthorhombic $KAlO_2$ phase can be described with a triclinic quasi-cubic subcell with dimensions close to those of the high-temperature cubic form (see the supplementary material[1]); moreover, the positions of the atoms in the subcell are close to those in the f.c.c. lattice (Fig. 3). The AlO_4 tetrahedra are located in the vertices and centers of faces, while K^+ ions are close to the subcell edges ($\angle$Al—K—Al $\simeq$ 177°). This framework model is similar to the cubic structure of cristobalite. The temperature dependence of the triclinic cell parameters shows a strong anisotropy which disappears at the othorhombic → cubic transition (Fig. 4). At this point (810 K), the conductivity increases ~2.5 times and reaches 10^{-3} S cm^{-1}, the activation energy decreases from 42 to 32.5 kJ mol^{-1} (Burmakin *et al.*, 2004), while the unit-cell volume dependence is monotonous (Table 1, Fig. 5). So we have no reason to attribute the jump-like increase of the conductivity to the lattice thermal extension. At the same time, the Debye–Waller factors for Al and K atoms significantly increase at the phase transition point (Fig. 6). On the other hand, the neutron diffraction patterns contain sharp peaks of the cubic phase after the othorhombic → cubic

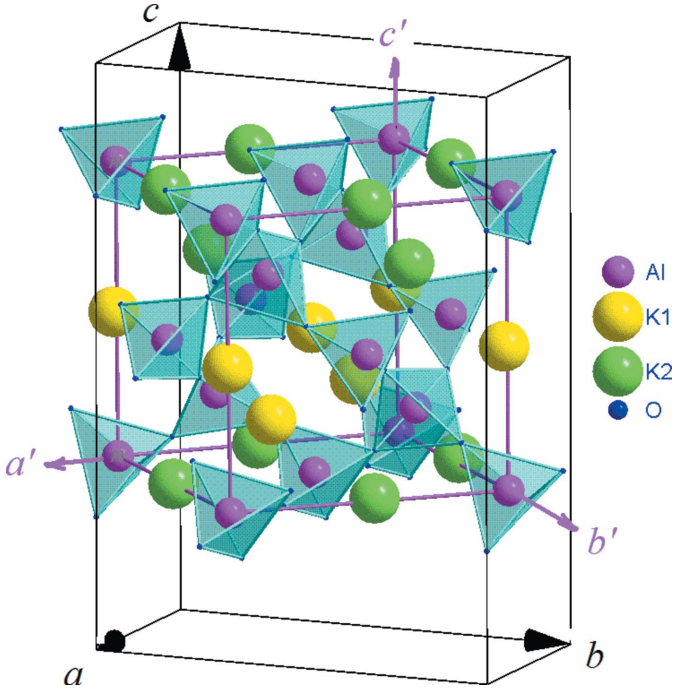

Figure 3
Position of the triclinic quasi-cubic subcell (a', b', c') in relation to the orthorhombic cell (a, b, c).

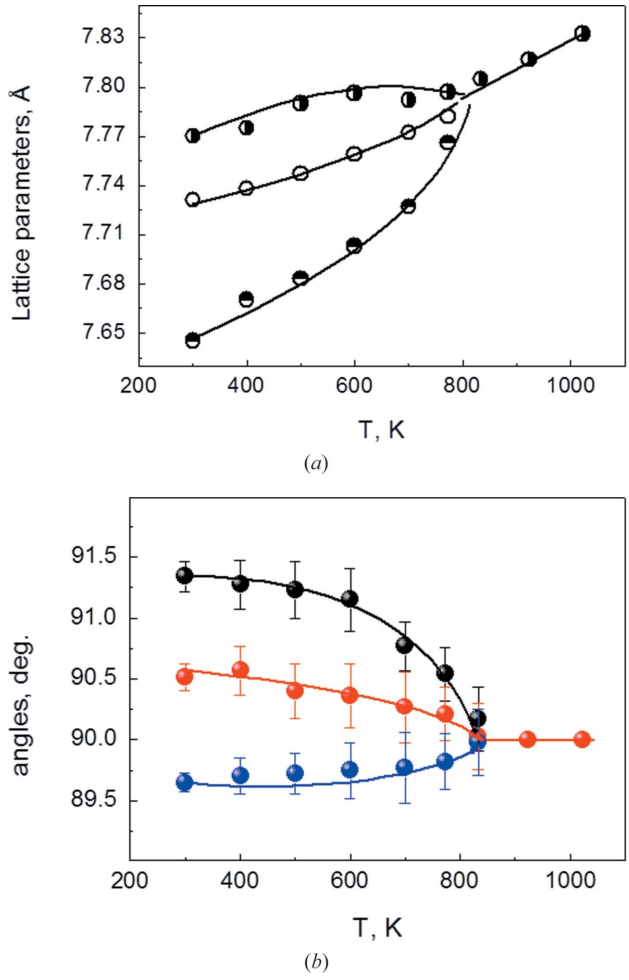

Figure 4
Temperature dependence of (*a*) linear and (*b*) angular parameters of the triclinic sublattice of $KAlO_2$.

[1] Supplementary data for this paper are available from the IUCr electronic archives (Reference: KD5061). Services for accessing these data are described at the back of the journal.

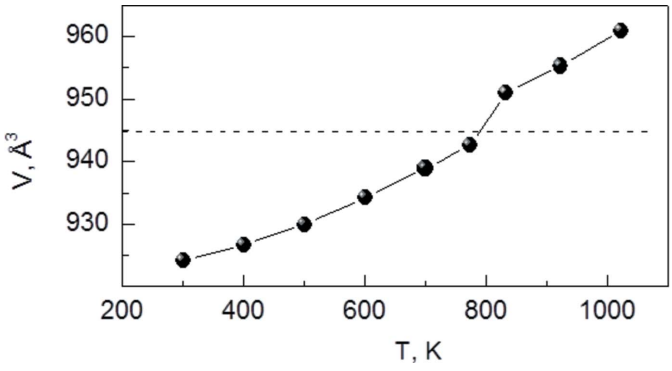

Figure 5
Temperature dependence of the unit-cell volume for the orthorhombic and cubic $KAlO_2$ phases. For the cubic phase the volume is doubled to fit the number (8) of formula units for the orthorhombic phase.

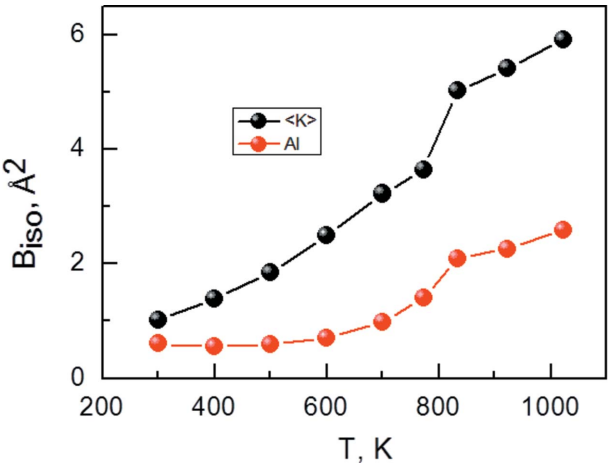

Figure 6
Temperature dependences of the Debye–Waller factors for Al and K atoms in $KAlO_2$.

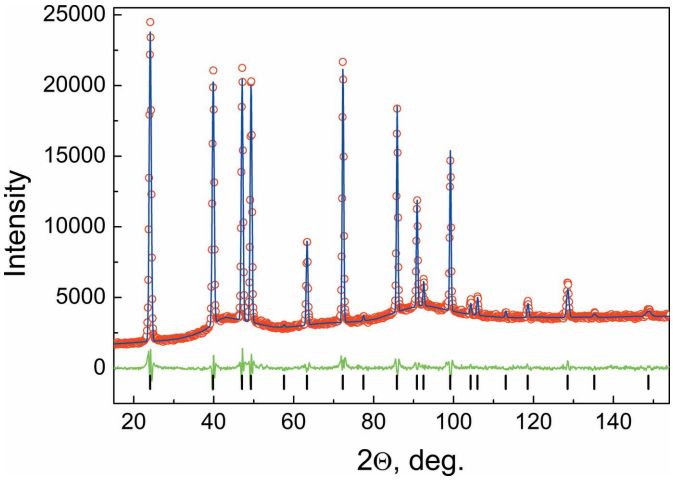

Figure 7
Fitted powder neutron diffraction profile for $KAlO_2$ at 1073 K with observed (dots), calculated (solid line) and difference plots. Dashes designate the angular positions of the reflections.

transition, but broad diffuse maxima appear instead of the isotropic background (Fig. 7) that is typical for amorphous and liquid materials. For K^+ cations the thermal factor value is ~ 5.0 Å^2 after the transition that corresponds to the oscillation amplitude of ~ 0.5 Å or $\sim 15\%$ of the K—K distance (~ 3.4 Å). According to Lindemann's criterion (Lindemann, 1910; Hansen & Verlet, 1969), such an increase of the vibrational amplitudes is comparable with that at the melting point. This gives evidence of the essential disordering of the K^+ cations.

3.2. Relations between the $KAlO_2$ crystal structure features and K^+ conductivity

The *TOPOS* analysis of dual nets reveals five non-equivalent elementary channels (I)–(V) in the K^+ migration map of the low-temperature phase. These channels correspond to five non-equivalent framework windows and differ in size (Table 2) and form (Fig. 8). They also play different roles in the migration map (Fig. 9): windows (V) form channels [100] that provide the conductivity at low temperatures (Vielhaber &

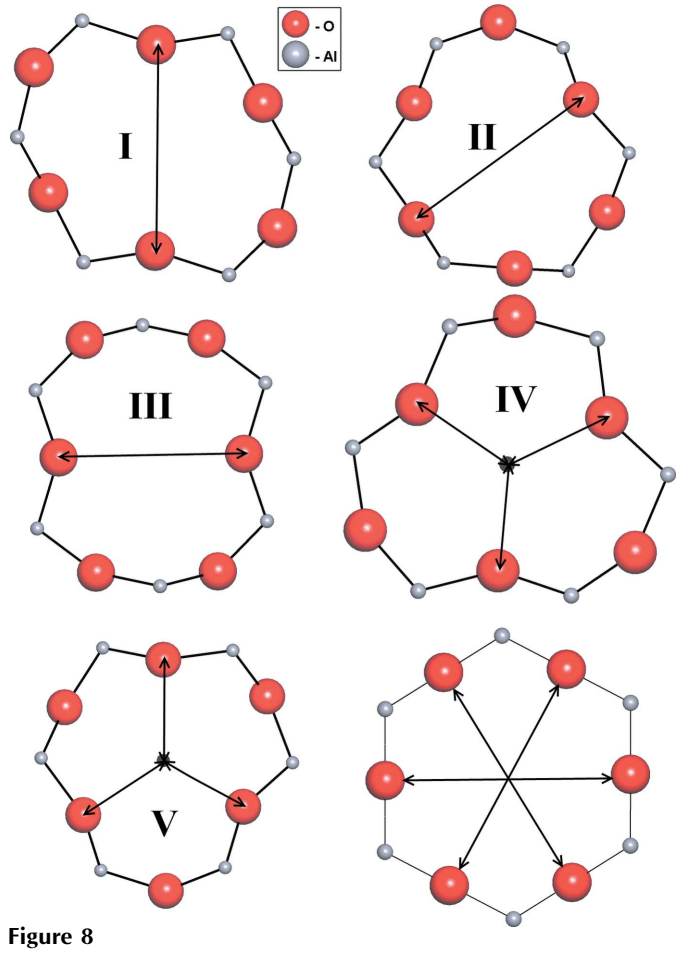

Figure 8
Non-equivalent windows in low-temperature $KAlO_2$ (I)–(V) and (bottom right) the window in high-temperature $KAlO_2$. The arrows show the methods of computing radii: for windows (I)–(III) the radius is equal to the half distance between the closest opposite O atoms; for windows (IV) and (V) it is estimated as the radius of the sphere inscribed into the window.

Hoppe, 1969; Fig. 9 top); windows (I) and (II) connect the channels into a layer (010) system, which is extended to a three-dimensional net through windows (III) and (IV) (Fig. 9 bottom). The sizes of the windows were estimated depending on their form: for windows (I)–(III) there are two O atoms close to the center of the window, while for windows (IV) and (V) there are three such atoms (Fig. 8). Assuming r_{min} = 2.30 Å (Voronin *et al.*, 2010), the low-temperature $KAlO_2$ conductivity is expected to be anisotropic, since only elementary channels (I), (II) and (V) remain significant. The elementary channels (III) and (IV) correspond to narrower windows that are less accessible for mobile potassium cations. This result in general confirms the conclusions drawn with the Voronoi–Dirichlet method (Voronin *et al.*, 2010), where the conductivity was predicted to be anisotropic and channels [100] were considered as the most probable paths of cation migration. At the same time, the tiling method gives a two-dimensional migration pattern, while the Voronoi–Dirichlet method predicts a one-dimensional system of accessible channels. Taking into account the aforesaid advantages of the tiling method, the two-dimensional migration pattern seems more reasonable.

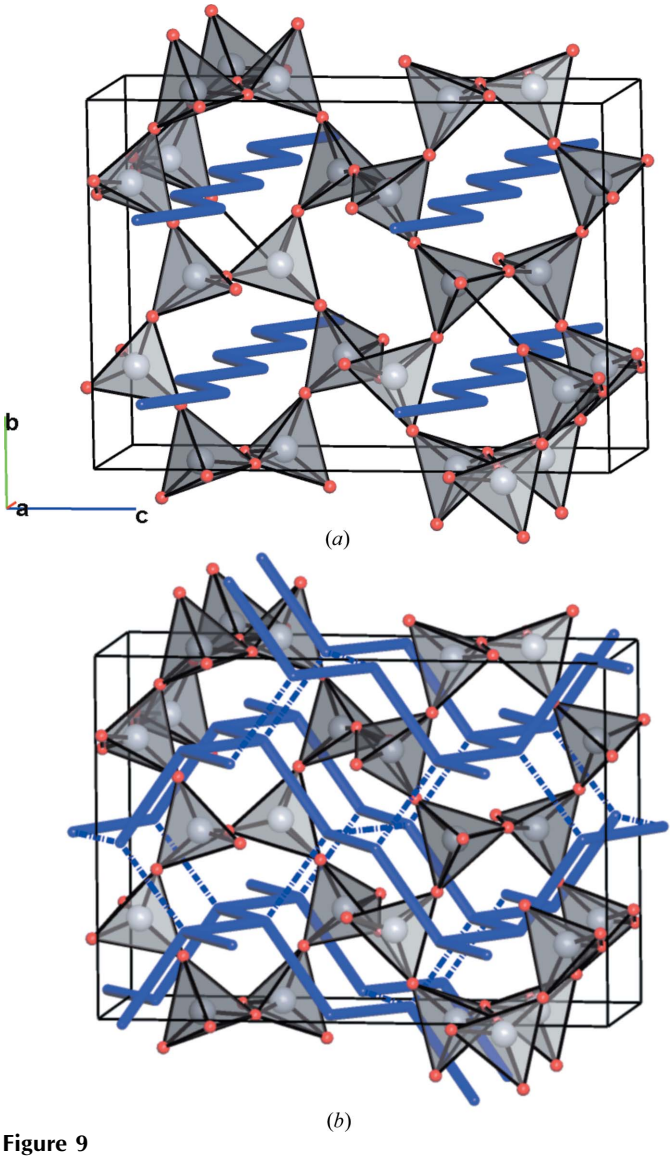

Figure 9
The orthorhombic $KAlO_2$ phase at 300 K. (*a*) The channels [100] passing through windows (V); (*b*) the layer channel systems (010) with participation of windows (I) and (II) as well as additional narrow channels (dashed lines) passing through windows (III) and (IV).

Table 2
Radii of framework windows (I)–(V) (Å) in orthorhombic and cubic $KAlO_2$ phases at different temperatures.

E.s.d.'s for the windows sizes do not exceed 0.008 Å.

Temperature (K)	(I)	(II)	(III)	(IV)	(V)
300	2.392	2.505	2.180	2.241	2.412
400	2.417	2.505	2.201	2.251	2.417
500	2.436	2.496	2.217	2.266	2.447
600	2.451	2.508	2.256	2.291	2.467
700	2.489	2.512	2.295	2.308	2.483
773	2.532	2.512	2.347	2.350	2.522
833	2.758				
923	2.764				
1023	2.769				

As the temperature increases, the sizes of the windows become closer and during the orthorhombic–cubic phase transition increase dramatically to become identical after the transition (Fig. 10). It is important to take into account the quite monotonic increase of the unit-cell volume (Fig. 5). Such a cardinal difference in the temperature dependences of the cell volume and of the migration channel size during the phase transition is caused by a change of orientation of the AlO_4 tetrahedra. Fig. 11(*a*) shows that in the low-temperature form the tetrahedra are disoriented to each other and to the axes of the unit cell, so both the dimensions and the form of the migration channels are quite different. During the phase transition the tetrahedra rotate and become strongly ordered (Fig. 11*b*). This process gives rise to the drastic increase and equalization of the dimensions of the channels.

This dramatic reconstruction of the framework windows results in a high three-dimensional conductivity in the cubic phase. The topology of the framework is preserved in the cubic phase, however, thanks to a higher symmetry the tiling

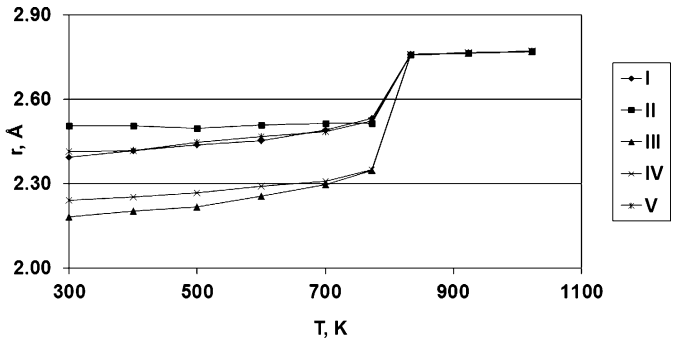

Figure 10
Temperature dependence of radii (*r*) of windows (I)–(V) in the orthorhombic and cubic $KAlO_2$ phases.

transitivity decreases to 1111 compared with 2452 for the orthorhombic phase. Hence, the cubic phase has only one independent elementary channel in the migration map with a radius increasing from 2.758 to 2.769 Å at high temperature (Fig. 10). The channel sections are round compared with corrugated channels in the orthorhombic phase (Fig. 8); all O atoms bordering the channel are equidistant from its central line. The single non-equivalent window corresponds to the 6-ring of the diamond net (Fig. 2). Since the radius estimated as the distance from the channel central line to the centers of O atoms exceeds a typical K—O distance ($r_K + r_O = 1.33 + 1.36 = 2.69$ Å), potassium cations can move smoothly through the framework windows that give rise to the experimental high conductivity of cubic $KAlO_2$. In this case the migration map coincides with the dual net, *i.e.* all the elementary channels are significant.

4. Conclusion

Our analysis shows that the low-temperature orthorhombic $KAlO_2$ is a typical solid electrolyte with intrinsic thermal-activated defects in the whole range of existence. The conductivity is highly anisotropic as two of five types of elementary migration channels are of small size and remain inaccessible to the K^+ cations. The structural phase transition to the f.c.c. form is followed by a decrease in the conductivity activation energy, which indicates increased mobility of the current carriers. The main reasons for this increase are enlargement and equalization of the elementary channels. As a result, the K^+ cations can move along all the channels with minimal hindrances that should give rise to a decrease of the conductivity anisotropy. The results obtained give evidence of the efficiency of the natural tiling approach for analyzing the conducting properties of anionic frameworks. In accordance with this approach, an infinite migration map is divided into elementary channels following a strict algorithm (Blatov *et al.*, 2007); the number of independent elementary channels is always finite and, as a rule, does not exceed 10–20, simplifying the migration pattern analysis. The tiling approach reveals advantages in comparison with the Voronoi–Dirichlet method (Anurova *et al.*, 2008; Voronin *et al.*, 2010) as we were able to study in detail the temperature dependence of migration maps and their transformations during the othorhombic → cubic phase transition.

Despite the favourable structural changes at the orthorhombic → cubic transition, the conductivity of high-temperature $KAlO_2$ is not very large ($\sim 10^{-3}$ S cm^{-1}). The reason could be in a small number of vacant positions in the potassium sublattice. This is confirmed by a sharp increase of the conductivity in the $KAlO_2$ samples where the Al^{3+} cations are partially substituted for four-charged cations (Burmakin *et al.*, 1979; Burmakin, 1992).

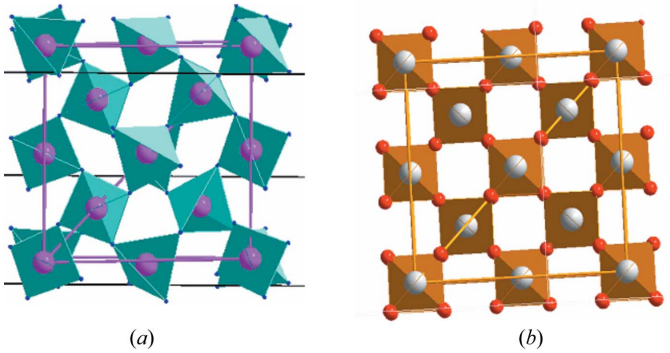

(*a*) (*b*)

Figure 11
Spatial orientation of AlO_4 tetrahedra in (*a*) the low-temperature and (*b*) the high-temperature phase of $KAlO_2$.

This work is supported by Russian Foundation for Basic Research (grant No. 03-11-00663) and Program No. 16.518.11.7032 of Russian Ministry of Education and Science.

References

Ali, N. Z., Nuss, J., Sheptyakov, D. & Jansen, M. (2010). *J. Solid State Chem.* **183**, 752–759.
Anurova, N. A. & Blatov, V. A. (2009). *Acta Cryst.* B**65**, 426–434.
Anurova, N. A., Blatov, V. A., Ilyushin, G. D., Blatova, O. A., Ivanov-Schits, A. K. & Dem′yanets, L. N. (2008). *Solid State Ionics*, **179**, 2248–2254.
Avdeev, M., Nalbandyan, V. B. & Shukaev, I. L. (2009). *Solid State Electrochemistry: Fundamentals, Methodology and Applications*, edited by V. V. Kharton. Weinheim: Wiley-VCH.
Barth, T. F. W. (1935). *J. Chem. Phys.* **3**, 323–325.
Bertaut, E. F., Delapalme, A., Bassi, G., Durif-Varambon, A. & Joubert, J. C. (1965). *Bull. Soc. Fr. Mineral. Crist.* **88**, 103–108.
Blatov, V. A. (2006). *IUCr CompComm Newsl.* **7**, 4–38.
Blatov, V. A., Delgado-Friedrichs, O., O'Keeffe, M. & Proserpio, D. M. (2007). *Acta Cryst.* A**63**, 418–425.
Blatov, V. A., Ilyushin, G. D., Blatova, O. A., Anurova, N. A., Ivanov-Schits, A. K. & Dem'yanets, L. N. (2006). *Acta Cryst.* B**62**, 1010–1018.
Brownmiller, L. T. (1935). *Am. J. Sci.* **29**, 260–277.
Burmakin, E. I. (1992). *Solid Electrolytes with Alkali Ion Conductivity*. Moskow: Nauka (in Russian).
Burmakin, E. I., Burov, G. V., Rozanov, I. G. & Shekhtman, G. Sh. (1978). *Russ. J. Inorg. Chem.* **23**, 3366–3368.
Burmakin, E. I., Shekhtman, G. Sh. & Stepanov, G. K. (1979). *Dokl. Akad. Nauk SSSR*, **244**, 1374–1378.
Burmakin, E. I., Voronin, V. I., Akhtyamova, L. Z., Berger, I. F. & Shekhtman, G. Sh. (2004). *Russ. J. Electrochem.* **40**, 619–625.
Burmakin, E. I., Voronin, V. I., Akhtyamova, L. Z., Berger, I. F. & Shekhtman, G. Sh. (2005). *Russ. J. Electrochem.* **41**, 783–788.
De Kroon, A. P., Schäfer, W. & Aldinger, F. (2001). *J. Alloys Compd.* **314**, 147–153.
Fischer, P., Frey, G., Koch, M., Konnecke, M., Pomjakushin, V., Schefer, J., Thut, R., Schlumpf, N., Burge, R., Greuter, U., Bondt, S. & Berruyer, S. (2000). *Physica B*, **276–278**, 146–147.
Hansen, J.-P. & Verlet, L. (1969). *Phys. Rev.* **184**, 151–161.
Husheer, S. L. G., Thompson, J. G. & Melnichenko, A. (1999). *J. Solid State Chem.* **147**, 624–630.
Kaduk, J. A. & Pei, S.-Y. (1995). *J. Solid State Chem.* **115**, 126–139.
Langlet, G. (1964). *C. R. Hebd. Seances Acad. Sci.* **259**, 3769–3770.
Lindemann, F. A. (1910). *Z. Phys.* **11**, 609–612.
Marezio, M. (1965). *Acta Cryst.* **19**, 396–400.
Müller, M., Dinnebier, R. E., Ali, N. Z., Campbell, B. J. & Jansen, M. (2010). *Mater. Sci. Forum*, **165**, 79–95.
Pistorius, C. W. F. T. & de Vries, G. F. (1973). *Z. Anorg. Allg. Chem.* **395**, 119–121.
Rodriguez-Carvajal, J. (1993). *Physica B*, **192**, 55–69.

Shannon, R. D. (1976). *Acta Cryst.* A**32**, 751–767.
Sheptyakov, D., Ali, N. Z. & Jansen, M. (2010). *J. Phys. Condens. Matter*, **22**, 426001.
Sokolowski, J. & Kotarba, A. (2000). *Mater. Sci. Forum*, **321–324**, 954–959.
Vielhaber, E. & Hoppe, R. (1969). *Z. Anorg. Allg. Chem.* **369**, 14–32.
Voronin, V. I., Surkova, M. G., Shekhtman, G. Sh., Anurova, N. A. & Blatov, V. A. (2010). *Inorg. Mater.* **46**, 1234–1241.
West, A. R. (1995). *Solid State Electrochemistry*, edited by P. J. Bruce. Cambridge University Press.